Amyloid properties of the leader peptide of variant B cystatin C: implications for Alzheimer and macular degeneration

Ricardo Sant'Anna[1], Susanna Navarro[1], Salvador Ventura[1], Luminita Paraoan[2] and Debora Foguel[3]

1 Institut de Biotecnologia i Biomedicina and Departament de Bioquímica i Biologia Molecular, Universitat Autònoma de Barcelona, Bellaterra, Spain
2 Department of Eye and Vision Science, Institute of Ageing and Chronic Disease, University of Liverpool, UK
3 Instituto de Bioquímica Médica Leopoldo de Meis, Programa de Biologia Estrutural, Universidade Federal do Rio de Janeiro, Brazil

Correspondence
D. Foguel, Instituto de Bioquímica Médica Leopoldo de Meis, Programa de Biologia Estrutural, Universidade Federal do Rio de Janeiro, Rio de Janeiro, 21941-901 Brazil
Fax: +552122708647
Tel: +552139386761
E-mail: foguel@bioqmed.ufrj.br

S. Ventura, Institut de Biotecnologia i Biomedicina, Universitat Autònoma de Barcelona, Bellaterra L69 3BX, Spain
Fax: +34 93 581 2011
Tel: +34 93 586 8956
E-mail: salvador.ventura@uab.es
and
L. Paraoan, Department of Eye and Vision Science, Institute of Ageing and Chronic Disease, University of Liverpool, Liverpool 08193, UK
Fax: +44 151 795 8420
Tel: +44 151 794 9038
E-mail: lparaoan@liverpool.ac.uk

Variant B (VB) of cystatin C has a mutation in its signal peptide (A25T), which interferes with its processing leading to reduced secretion and partial retention in the vicinity of the mitochondria. There are genetic evidences of the association of VB with Alzheimer's disease (AD) and age-related macular degeneration (AMD). Here, we investigated aggregation and amyloid propensities of unprocessed VB combining computational and *in vitro* studies. Aggregation predictors revealed the presence of four aggregation-prone regions, with a strong one at the level of the signal peptide, which indeed formed toxic aggregates and mature amyloid fibrils in solution. In light of these results, we propose for the first time the role of the signal peptide in pathogenesis of AD and AMD.

Keywords: Alzheimers' disease and exudative age-related macular degeneration; human cystatin C; protein aggregation

Highlights
- Variant B precursor of the cysteine proteinase inhibitor cystatin C has been previously associated with increased risk of developing Alzheimer's disease (AD) and exudative age-related macular degeneration (AMD).
- We show here that the leader sequence of the variant B precursor cystatin C presents high aggregation and amyloidogenic propensity.
- Retention of the leader sequence in the incompletely processed variant can contribute to deleterious protein aggregation linked to pathogenesis of AD and AMD.

Human cystatin C belongs to the cystatin superfamily of reversible inhibitors of cysteine proteases encompassing the papain and legumain families [1]. The mature cystatin C is a monomeric protein composed of a polypeptide chain of 120 amino acids (13 343 Da) [2,3]. The general fold of monomeric inhibitors of the cystatin
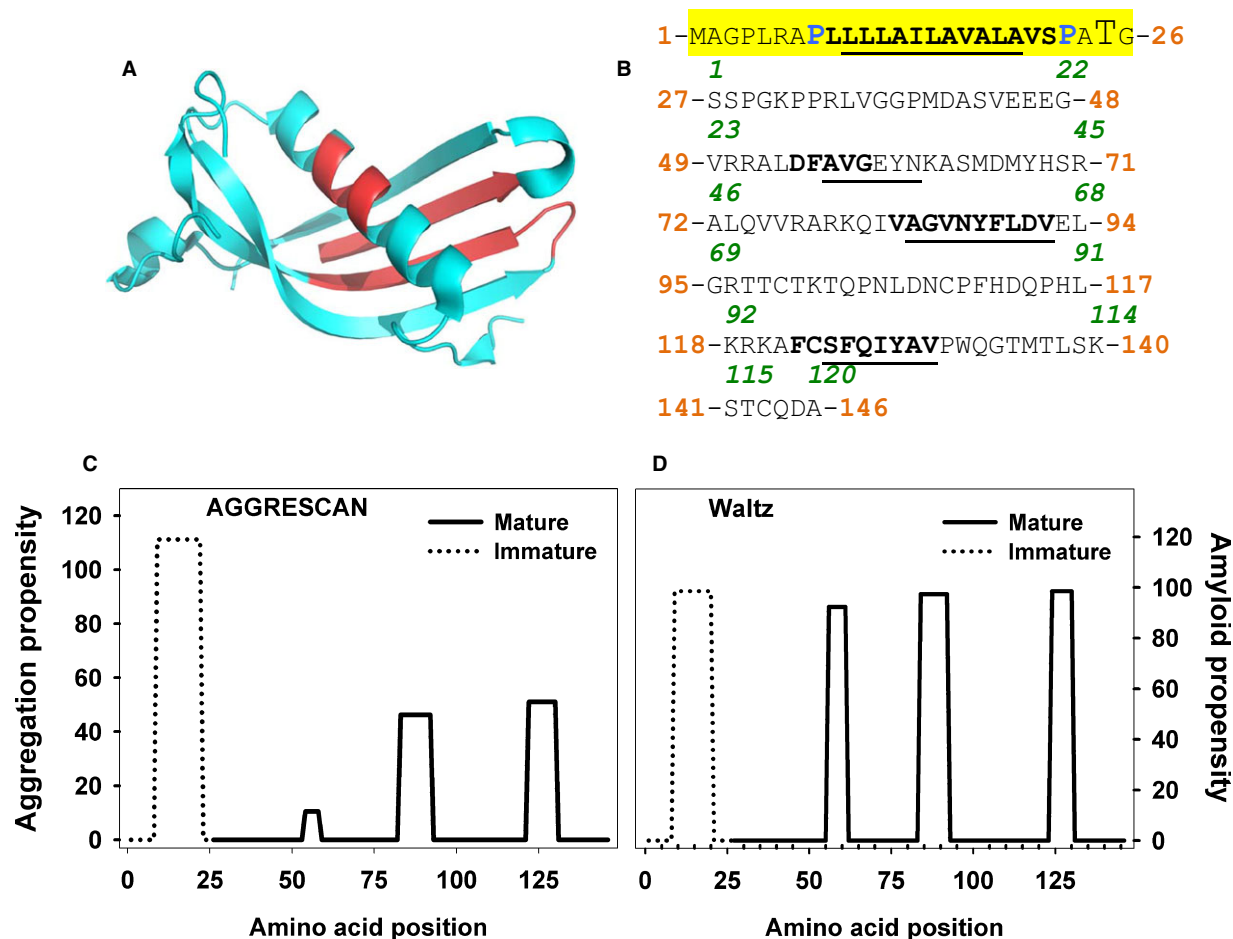
Fig. 1. Tridimensional structure, primary sequence and *in silico* aggregation and amyloid propensity predictions for WT and variant B cystatin C. (A) A monomer-stabilized human cystatin C with an engineered disulfide bond (PDB ID: 3GAX) [61] reveals the canonical cystatin fold, based on the crystal structure of chicken cystatin [62]. In red are the regions pointed out by AGGRESCAN as the aggregation-prone regions in the protein. (B) The amino acid sequence of the variant B precursor cystatin C with the aggregation-prone regions (APR) identified by AGGRESCAN in bold and by Waltz underlined. The leader peptide is highlighted in yellow. Gatekeeper residues flanking APR of the signal peptide are in blue. We are using two numerations, the orange numbering includes the signal peptide and contains 146 residues, the green numeration corresponds to the processed cystatin C, which contains 120 residues. In (C), the aggregation propensity of both sequences was predicted using AGGRESCAN (http://bioinf.uab.es/aggrescan/) using default parameters. (D) The same procedure was used to predict the amyloid propensity by the algorithm Waltz (http://www.switchlab.org/bioinformatics/waltz). We call attention to the fact that continuous lines (mature cystatin C) are superimposed to the dashed lines (immature cystatin C).

superfamily has been defined by the crystal structure of chicken cystatin. It is composed of a long helix running across a five-stranded antiparallel β-sheet [3,4] (Fig. 1A). Cystatin C is produced and found in most tissues and body fluids with particular higher concentrations in the cerebrospinal fluid, owing to expression by the choroid plexus. Cystatin C is involved in many biological functions, ranging from bone reabsorption, modulation of inflammatory response, antiviral and antibacterial properties, cell proliferation and growth, tumor metastasis, and to astrocyte differentiation during mouse brain development [5–9].

Wild-type (WT) cystatin C has been found in amyloid deposits in the brain arteries of elderly people [10,11], while the rare mutation L68Q causes hereditary cystatin C amyloid angiopathy (HCCAA) [12,13], a condition in which the patients present fatal cerebral hemorrhage in early adulthood. *In vitro*, both WT and L68Q cystatins C produce amyloid fibrils [12,14,15]. Interestingly, *in vitro* and *in vivo* studies have shown that WT cystatin C binds to soluble Aβ protecting this peptide from oligomerization. In addition, cystatin C has been colocalized with Aβ deposits in senile plaques and the vascular cell wall. Altogether, these results suggest that mature cystatin C might

be a neuroprotective protein in Alzheimer's disease (AD) acting as a modulator of amyloidosis [16–18].

In the eye, cystatin C is abundantly expressed by the retinal pigment epithelium (RPE) [19–21], the monolayer of cells essential for maintaining the homeostasis of the neuroretina and the blood–retina barrier. RPE dysfunction is central to the pathogenesis of age-related macular degeneration (AMD), with various cellular processes contributing to the onset and progression of the disease including: cellular debris accumulation in drusen [22], changes to the underlying Bruch's membrane (BM) with and without breakage of the blood/retina barrier [23], impaired clearing of protein aggregates and/or damaged organelles [24,25].

The cystatin C variant type B has been associated as a recessive allele with increased risk of AD and exudative AMD [26–30]. This variant results from a SNP in the cystatin C gene (CST3) signal/leader sequence (1MAGPLRAPLLLLAILAVALAVSPAAG26) (p.Ala25Thr due to a c.G73A substitution). The 26-amino acid signal sequence of precursor cystatin C is essential for targeting the protein to the ER/Golgi apparatus and processing through the secretory pathway [31,32]. The A25T substitution decreases the efficiency of cleavage of the signal peptide in the variant B precursor resulting in a protein constituted of 146 amino acids that is abnormally processed in the cell [33]. The variant B precursor cystatin C is processed less efficiently through the secretory pathway resulting in its decreased secretion to the extracellular space, with some of the unprocessed molecules diverted from the secretory pathway accumulating intracellularly in association with the mitochondrial membrane network [33,34]. The reduced secretion and subsequent decreased concentration of mature cystatin C extracellularly could explain the enhanced AD and AMD risk observed in homozygous patients with variant B.

Here, due to its association with AD and AMD, we investigate the aggregation and amyloid propensity of the variant B, with emphasis on the signal peptide. Using two well validated aggregation predictors, namely AGGRESCAN, which was designed to predict aggregation propensity regions *in vivo*, and Waltz, which predicts specific amyloid formation regions [35,36], we found on the immature form of the protein, four short aggregation-prone sequences, one of them being the leader peptide with very high aggregation/amyloidogenic scores. With these predictions in hands, we carried out *in vitro* experiments with the leader peptide to corroborate its amyloidogenicity. Our data unequivocally demonstrated that the leader peptide of the variant B cystatin C aggregates instantaneously upon aqueous dilution forming positive Thioflavin-T

(Th-T) and Congo red aggregates. ATR-FTIR, TEM and DLS confirmed the presence of amyloid in solution. The aggregates were shown to be very toxic to neuroblastoma cells cultures. In light of these results, we propose for the first time a role of the leader peptide on the immature (unprocessed) form of variant B cystatin C in its association with increased risk of AD and AMD.

Materials and methods

Prediction of the peptide aggregation and amyloid propensities

AGGRESCAN, Waltz, TANGO and Zipper DB Analysis – The intrinsic aggregation and amyloid formation propensities of mature and immature cystatin C were evaluated by these four methods employing default settings, using as input the primary sequence of either the mature protein or the immature form of variant B cystatin C. Uniprot Accession Number P01034 (CYTC_HUMAN) and the dbSNP Classification code rs1064039 [*Homo sapiens*].

Peptides synthesis

The peptides were purchased from CASLO ApS c/o Scion Denmark Technical Universit (Lyngby, Denmark). The purity was higher than 98%. The peptide was weighted and diluted in DMSO to obtain a stock solution of soluble peptide with a concentration of 3 mM.

Peptides aggregation assays

Aggregation was performed at different concentrations as stated in legends. Before each experiment, the stock solution was diluted in PBS pH 7.4 and Th-T was added at 20 μM (Fig. 2B) or 30 μM (Fig. 2A) final concentrations. The samples were incubated at 25 °C with no agitation. Samples were excited at 450 nm while emission was collected from 400 to 600 nm on a spectrofluorometer Jasco 8200. Intensity at 482 nm was used to probe amyloid formation.

Congo red binding assay

The binding of CR to aggregated peptide was evaluated by diluting fivefold the incubated peptide in CR, resulting in a final CR concentration of 10 μM, and recording the absorbance spectra of the mixture in the 380–670 nm range in a Cary 400 spectrophotometer (Varian, Palo Alto, CA, USA).

Dynamic light scattering measurements

Peptide solutions were let to aggregate at the conditions stated above (100 μM) and measures were performed at 1 h
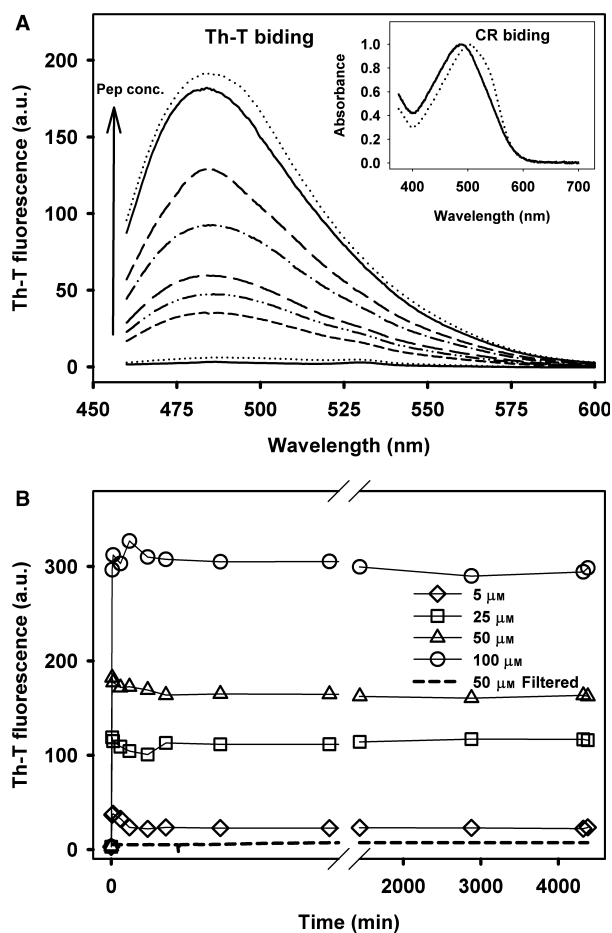
Fig. 2. Monitoring aggregation of variant B cystatin C signal peptide *in vitro*. Panel A: Increasing concentrations of the signal peptide (5–100 μM, as indicated) were incubated in PBS (pH 7.4) at 25 °C without agitation (aggregation condition). After 1 h under this condition, Th-T binding was evaluated by measuring its fluorescence emission (Excitation = 450 nm and Emission = 450–600 nm). [Th-T] = 20 μM. The inset in Panel A shows the spectra of CR alone and in the presence of aggregates formed after 24 h of incubation. Panel B displays the kinetics of aggregation at different concentrations of the signal peptide (see the legend inside this panel) as followed by the intensity of Th-T fluorescence at 482. [Th-T] = 30 μM.

and after 24 h of aggregation. DLS measurements were performed at 25 °C in a Malvern Zetasizer Nano S90 (Malvern, Worcestershire, UK). Each sample was measured tree times; average distributions are presented.

Infrared spectroscopy

Attenuated total reflectance Fourier transform infrared spectroscopy (ATR-FTIR) was used to determine the secondary structure content of the aggregates formed at different times during the aggregation kinetics. The experiments

were carried out using a Bruker Tensor 27 FTIR spectrometer (Bruker Optics, Billerica, MA) with a Golden Gate MKII ATR accessory. Each spectrum consists of 16 accumulations measured at a resolution of 2 cm^{-1} in a wavelength range between 1700 and 1600 cm^{-1}. Infrared spectra were fitted through overlapping Gaussian curves, and the amplitude, mass center, bandwidth at half of the maximum amplitude and area for each Gaussian function were calculated employing a nonlinear peak-fitting equation using the PEAKFIT package (Systat Software, San Jose, CA, USA).

Transmission electron microscopy

Aggregated samples were diluted in Mili-Q water to 10 μM. Five microliter of the solution was absorbed onto carbon-coated copper grids for 5 min and blotted to remove excess material. Uranyl acetate (2% w/v) was used for negative staining. Samples were dried on air for 5 min. Grids were exhaustively scanned with a Hitachi H-7000 transmission electron microscope operating at a voltage of 75 kV.

Neuroblastoma cell (N2a) culture and viability assay

Neuroblastoma cells (N2a) were cultured in Dulbecco's modified Eagle's medium supplemented with 10% fetal bovine serum and 2% antibiotic (gentamicin) in a 5% CO_2 atmosphere for 3 days and then transferred to a 96-well plate and allowed to adhere for 24 h (5000 cells per well). Following cell adhesion, aggregates were added to achieve final concentration of 5 μM. Cells were challenged for 24 h, and final cellular viability was measured by an MTT assay as previously described [37].

Results and Discussion

Bioinformatics predicts that the signal peptide of variant B cystatin C is aggregation prone and amyloidogenic

AGGRESCAN is considered a reliable program to predict the aggregation propensity of proteins *in vivo* [38] as the aggregation score for each amino acid was derived from aggregation assays carried out on a bacterial system [35]. AGGRESCAN identifies aggregation-prone regions (APR) as stretches of a given sequence at least five amino acids long with high aggregation propensity scores [39].

Recently, the pentapeptide [47]LQVVR[51] from cystatin C was demonstrated to form fibrils *in vitro* [40]. The same group by using the algorithm AMYLPRED identified two other peptides from the core of cystatin C with high aggregation propensity. These peptides, namely [56]IVAGVNYFLD[65] and [95]AFASFQIYAV[104]

(it contains a C97A mutation), were also amyloido-
genic upon incubation for several days at pH 5.5.
These peptides numberings are from the mature cys-
tatin C. In our Fig. 1B, green numbering [41].

Figure 1C shows the aggregation propensity scores
as predicted by AGGRESCAN for the immature (variant B)
and mature forms of cystatin C. As seen, according to
this algorithm, the mature protein contains three APRs
located at positions 54–58 (DFAVG), 83–92 (VAGV-
NYFLDV) and 122–130 (FCSFQIYAV) (immature
form numbering, orange numbering on Fig. 1B). The
regions 83–89 and 122–130 in the immature form corre-
spond to residues 57–66 and 96–104 in the processed
protein (green numbering on Fig. 1B). Therefore, these
two APRs almost completely overlap with those previ-
ously identified using AMYLPRED [42].

Interestingly, the signal peptide present in the imma-
ture (uncleaved) protein (segment 9–22; LLLLAILA-
VALAVS) presented even higher aggregation scores
than the three previous peptides identified by AGGRES-
CAN. The primary sequence of precursor cystatin C,
including the signal peptide, is presented in Fig. 1B
and the aggregation-prone regions are highlighted.

APRs within the primary sequence of proteins are
flanked by gatekeeper residues such as proline and
charged amino acids, which modulate aggregation by
opposing nucleation of aggregates [43,44]. In the case
of the four stretches of cystatin C identified by AG-
GRESCAN, we could observe the presence of these gate-
keeper residues. In particular, in the case of the signal
peptide, the sequence is flanked by two proline resi-
dues at positions 8 and 23 (P-9LLLLAILAVA-
LAVS22-P). Recently, our group identified the
gatekeeper residues in the amyloidogenic protein
transthyretin. By replacing one of these residues in the
sequence of a peptide derived from TTR by a
hydrophobic amino acid (K35L), we could convert a
nonaggregating peptide into a highly aggregation-
prone one [45].

Next, in order to investigate whether these APRs
would also exhibit high scores for forming amyloid-
specific aggregates, the Waltz program was utilized
(Fig. 1D). As seen, all four segments of cystatin C,
including the signal peptide (segment 10–20 as pre-
dicted by this algorithm), presented propensity to form
amyloid assemblies. In this case, the other identified
regions with this property were 56–61 (AVGEYN),
84–92 (AGVNYFLDV) and 124–130 (SFQIIYAV)
(immature form numbering, orange numbering on
Fig. 1B). Both analyses were performed with the two
protein sequences, but as the only difference present
between them is the signal peptide, solid and dashed
lines appear superimposed.

We also used other algorithms such as TANGO
[46], Zipper DB [47] and AMYLPRED2 to analyze
the aggregation and amyloid propensity of the cystatin
C signal peptide. TANGO and AMYLPRED2 pre-
dicted the 9–20 and 9–21 stretches to be aggregation
prone, respectively, whereas Zipper DB predicted the
sequence 9–17 to be highly amyloidogenic. Because the
methods we employed here for computational predic-
tions rely on very different principles, the prediction of
the signal peptide being highly aggregation prone and
amyloidogenic was considered to be very robust. The
intrinsic high hydrophobicity of signal peptides does
not always implies that they can form typical beta
sheet rich ordered amyloid fibrils, as cystatin C signal
peptide does. To strengthen this very important point,
we ran Waltz for 20 signal peptides of different human
proteins randomly chosen from Uniprot (data not
shown). Interestingly, only 2 out of 20 presented
regions that could drive amyloid formation (Waltz
negative: P30453, P30483, Q9TNN7, P04114, P25774,
P08185, P16870, P11597, P28325, Q9UBU2, Q9NR61,
P16444, P54803, P47871, Q6UWU2, P42262; Waltz
Positive: Q8NFZ8, P12111).

Variant B cystatin C signal peptide is able to form amyloid fibrils *in vitro*

Having *in silico* evidence that the signal peptide pre-
sents high aggregation propensity and amyloidogenic-
ity, we synthesized the peptide with the mutation
A25T (1MAGPLRAPLLLLAILAVALAVSPATG26)
(Fig. 1B) and incubated it at increasing concentrations
(5–100 μM) for 1 h at pH 7.4, 25 °C under stagnant
conditions. As shown in Fig. 2A, there was a propor-
tional increase in Thioflavin-T (Th-T) emission at
increasing concentrations of the peptide, suggesting
formation of amyloid-like aggregates in solution.
Congo red (CR) binding assays were also performed
to confirm the presence of amyloid-like aggregates
(Fig. 2A, inset).

In order to follow the aggregation kinetics of the
signal peptide, increasing concentrations of the peptide
were incubated with Th-T and its fluorescence emis-
sion was collected over time (Fig. 2B). Notably, even
at very low peptide concentration such as 5 μM, maxi-
mum emission of Th-T was attained in the first acqui-
sition points, with no further change in the
fluorescence signal of the probe even after 3 days
under aggregation conditions. This suggests that aggre-
gation of the signal peptide of cystatin C is very fast.
We tried several conditions to slow down the aggrega-
tion process of the signal peptide such as low tempera-
ture (4 and 8 °C) and addition of 5, 10 and 15%
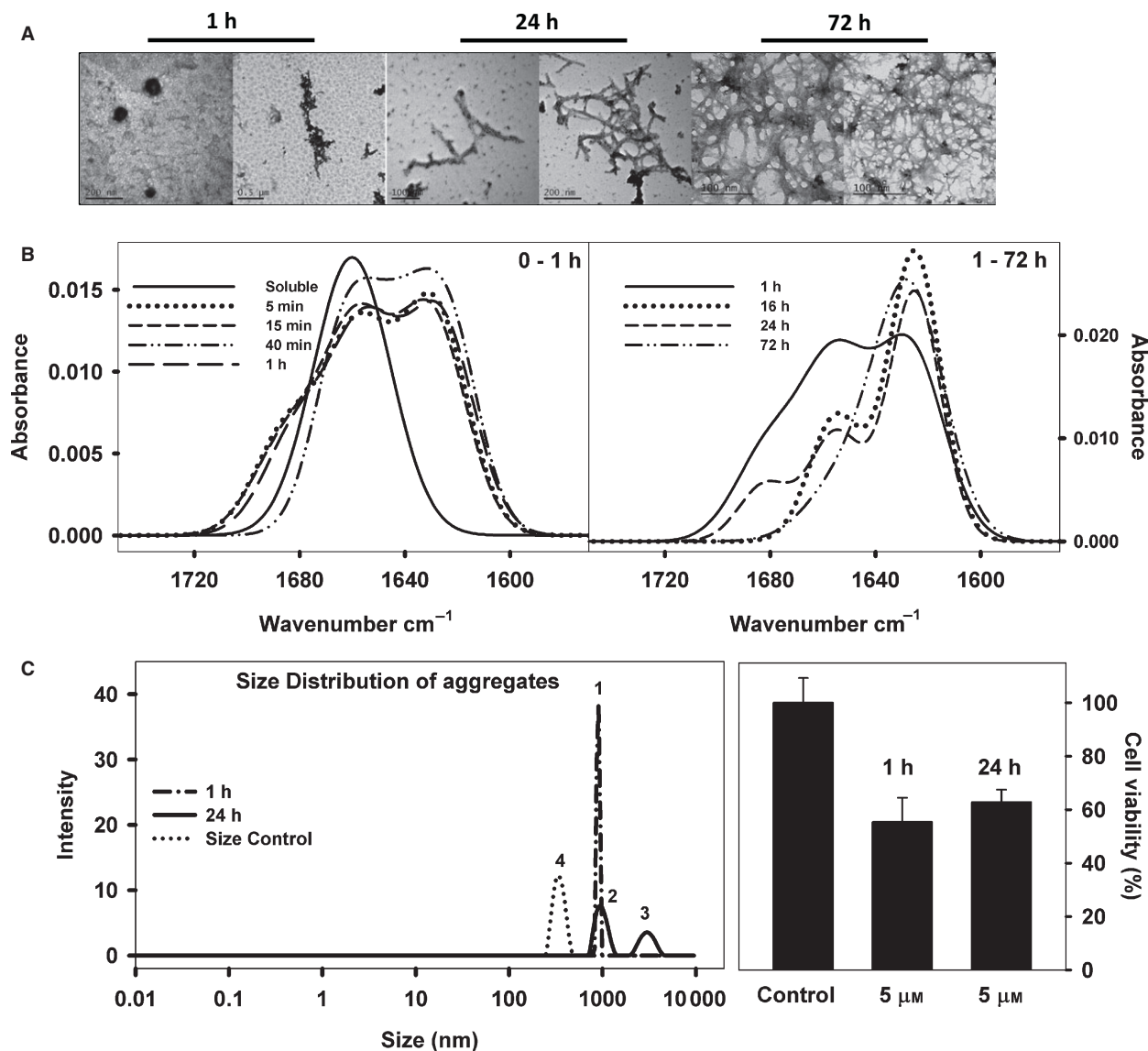
Fig. 3. Characterization of morphology, secondary structure content, size distribution and toxicity of the aggregates formed by the variant B cystatin C signal peptide. (A) Signal peptide at 100 μM was left to aggregate under the conditions described in Fig. 2. At 1 h (left images), 24 h (middle images) and 72 h (right images) aliquots were withdrawn and imaged by TEM. Bars represent 100, 200 and 500 nm. (B) Secondary structure changes that take place upon aggregation of the signal peptide analyzed by ATR-FTIR. The spectra displayed on the left side are those of the soluble peptide (full line), and of the samples aggregated up to 1 h as follows: 5 min (dotted), 15 min (short dash), 40 min (dash) and 60 min (large dash). On the right are displayed the FTIR spectra of the samples aggregated for longer times as follows: 1 h (full), 16 h (dot), 24 h (short dash) and 72 h (dash-dot). Secondary structure quantification from the deconvolution of these spectra is displayed in Table 1. (C) DLS was used to determine the size of the main species present at 1 h (dash-dot line) and 24 h (full line) under aggregating conditions. A calibration with silicone particles was performed and is shown in dotted line. (D) Toxicity of the aggregates formed at 1 and 24 h on neuroblastoma cells determined by MTT assay. In each case, 5 μM of aggregated material was added to the cells in culture remaining in contact with them for 24 h before cell viability evaluation.

DMSO to the aggregating buffer without any success (not shown).

In order to confirm the instantaneous aggregation of the signal peptide, a suspension with 50 μM peptide diluted into 30 μM Th-T was filtered through a 0.22 micrometer filter before measurements. The filter became yellow due to the retention of the aggregates bound to Th-T. The filtered solution, when let to aggregate, was not able to bind additional Th-T since all soluble peptide was converted into amyloid aggre-

gates that were retained in the filter (Fig. 2B, dashed line).

Characterizing the morphology, secondary structure and toxicity of the aggregates formed by the signal peptide of variant B cystatin C

Next, we used TEM to study the morphology of the species present at different times of aggregation (Fig. 3A). Interestingly, although Th-T binding has already leveled-off at 1 h under aggregation conditions, the great majority of the aggregated material presented an amorphous appearance and only few amyloid fibrils were observed at this time (Fig. 3A, left). The binding of Th-T to these amorphous species suggests that they already present cross-β fold able to accommodate this probe. These species are on-pathway to fibril formation since after 72 h under aggregation condition only mature fibrils were observed by TEM (Fig. 3A, right). At 24 h, it was already possible to see the presence of fibrils but small amorphous aggregates still remained (Fig. 3A, middle).

In order to get insights into the secondary structural changes that take place with the signal peptide upon aggregation, we took advantage of ATR-FTIR (Fig. 3 B). Left panel shows the FTIR spectra of the peptide dried from a stock solution with 100% DMSO (continuous line) and those collected during the first hour of aggregation. As seen, in DMSO the peptide presented a unique and broad peak centered at 1660 cm^{-1}, which corresponds to disordered, random-coiled structures, which is a strong evidence that the peptide is monomeric in DMSO [48–50].

At the initial times of aggregation (up to 1 h), the spectra changed and a new peak at 1628 cm^{-1} appeared which was assigned to β-sheet structures. At the same time, the peak related to random-coil structures (1660 cm^{-1}) decreased but was still present. The presence of β-sheet structures in these initial aggregates

explains why these species bind Th-T (as shown in Fig. 2), but they are not fully organized, as seen by TEM (Fig. 3A, left).

As aggregation proceeded for longer times (16, 24 and 72 h), the peak of β-sheet (1627 cm^{-1}) increased even further, with a concomitant decrease of the peak of random coil at 1660 cm^{-1}. Table 1 summarizes the secondary structural changes that take place upon aggregation of the signal peptide of cystatin C.

Next, to further confirm the difference in sizes of the species formed at 1 and 24 h, DLS measurements were performed (Fig. 3C). The main sizes of the two more prevalent species present at 1 h were 0.194 nm ± 0.06 nm and 904 ± 32.14 nm. After 24 h under aggregation conditions, there were two species present, one with 947 ± 134 nm and an extreme large species with 3008 ± 500 nm. Interestingly and corroborating the FTIR data, the species with around 900 nm were still present at 24 h. Given the fact that the aggregation pathways of aggregation-prone proteins are distinct leading to the accumulation of a myriad of aggregated species with different size and morphologies, it is difficult to make a direct comparison of the species sizes observed here with others. However, initial fibrillar species from Aβ peptide have been shown to have sizes from 200 to 700 nm [51,52]. In another study [53], the formation of transthyretin fibrillar oligomers of 1000 nm and mature fibrils with mean size of 4000 nm was reported [54], in accordance with our DLS data where early aggregating species with 900 nm and mature fibrils with 3000 nm were detected. We performed a calibration assay using a standard solution of silicone particles and the expected size was found (342 nm).
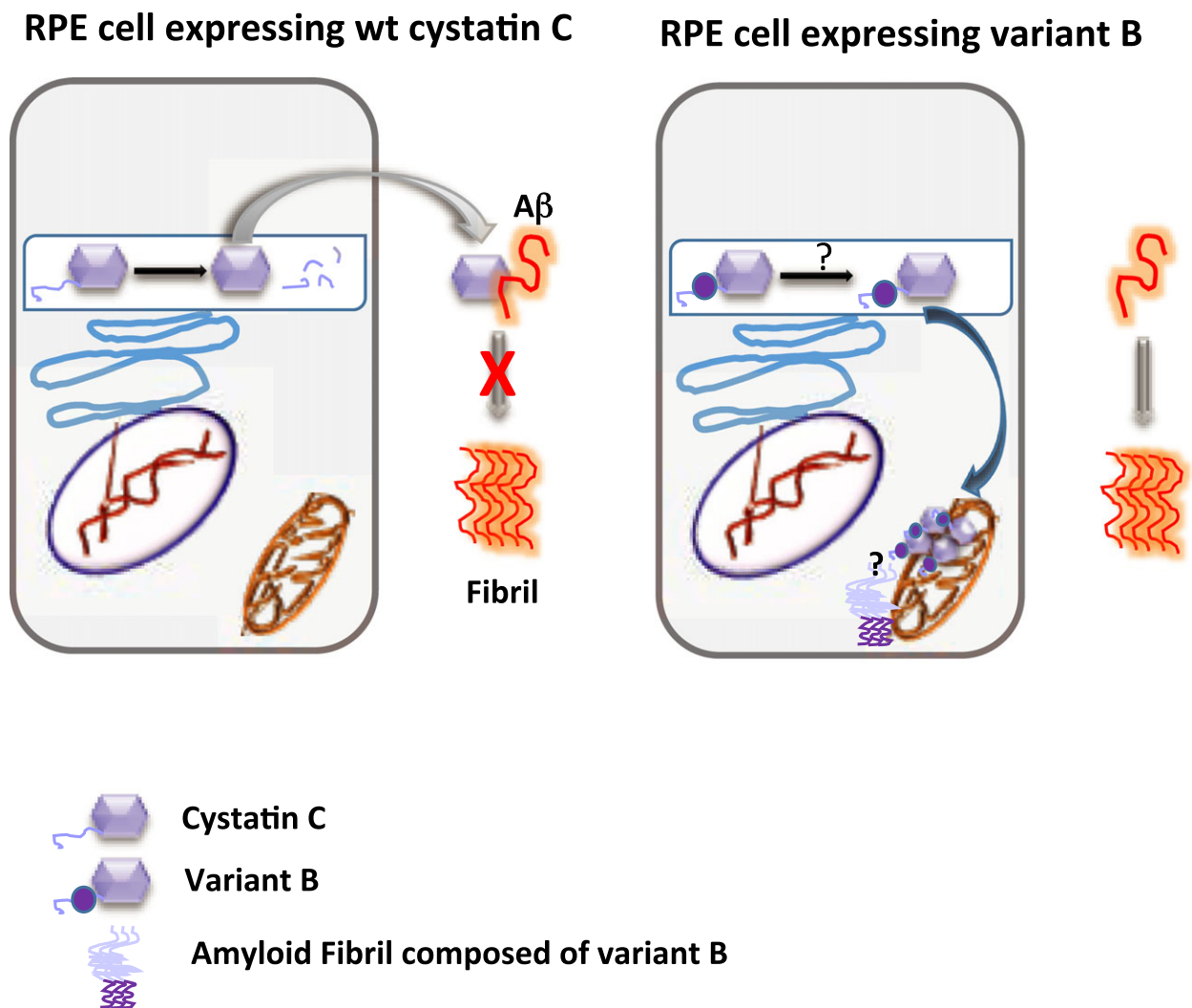
Next, neuroblastoma cell line N2a was used to probe the cytotoxicity of the aggregates formed at 1 and 24 h and cell viability was evaluated by MTT assays. Both aggregates tested at 5 μM concentration were very cytotoxic, killing ~ 40% of the cells (Fig. 3D).

Conclusions

The substitution A25T in the signal peptide of the variant B precursor cystatin C compromises its cleavage and/or processing precluding the efficient formation of the mature form of the protein, which is secreted from the cells to the extracellular milieu where it exerts its biochemical effect as a cysteine protease inhibitor. The variant leader presents a significant stretch of sequence with amyloidogenic propensity, which is even higher than the amyloidogenicsequences in the sequence of mature protein. This is relevant in the case when the leader is not cleaved thus imparting

Table 1. Secondary structure changes that take place upon aggregation of variant B cystatin C signal peptide measured by FTIR.

Time	Inter β-sheet (%) 1623–1641 cm^{-1}	Disordered (%) 1642–1657 cm^{-1}	β-sheet (%) 1674–1695 cm^{-1}
0	–	100	–
5 min	42.98	37.44	19.57
15 min	42.07	39.56	18.36
40 min	41.64	37.23	21.11
1 h	41.78	38.42	19.79
16 h	64.02	35.98	–
24 h	83.55	16.43	–
72 h	86.22	13.76	–

Fig. 4. Schematic representation of the effects of the A25T mutation on variant B precursor cystatin C cell trafficking and its possible implications for protein aggregation. On the left, a RPE cell that produces WT cystatin C. Processing of cystatin C takes place normally in the ER/Golgi network. The signal peptide is cleaved leading to the formation of the mature form of the protein, which is secreted from the RPE cells. Outside the cell, cystatin C acts as inhibitor of cysteine proteases. Besides, it can interact with Aβ modulating its aggregation properties. On the right, a RPE cell that produces the variant B, which is abnormally processed accumulating in the periphery of the mitochondria, probably as an aggregated material induced by the presence of the signal peptide. This variant is inefficiently secreted what impairs its protective effect against Aβ aggregation.

a higher amyloidogenic propensity to the full length variant precursor compared with the mature, processed protein. A model of the functional consequences for trafficking and protein aggregation of this variant precursor cystatin C is presented in Fig. 4. As previously shown, in the extracellular space mature cystatin C interacts with Aβ diminishing its aggregation [17,18]. An inefficiently cleaved/processed variant B cystatin C leads on one hand to a significantly reduced secretion of the mature cystatin C as shown previously [33,34] and, on the other, to the accumulation of full length variant precursor protein containing the mutated,

highly amyloidogenic leader. On the contrary, the WT signal peptide is efficiently excised from the normal cystatin C protein during its processing and should be completely cleaved. To our knowledge, there is no description of the accumulation/aggregation of the WT signal peptide inside RPE cells. In light of our data, it is tempting to suggest that this variant might aggregate into amyloid fibrils through the leader peptide, since the other stretches with high aggregation propensity are protected in the globular domain of the protein. These aggregates composed of uncleaved/unprocessed variant B could be formed either inside or

outside the cells leading to a gain of toxic function. As previously demonstrated [34] this variant is retained close to mitochondria walls forming structures resistant to protease digestion [34], a characteristic feature of high molecular weight aggregates, including amyloid fibrils. Upon aggregation of variant B, other important intra- or extracellular protein components could be incorporated into this aggregated material, possibly depriving the cell/tissue from a specific function and forming protein aggregates otherwise not present in the cells. Additionally, lower levels of functional mature cystatin C in the extracellular space could be very deleterious, contributing to increased proteolytic action at its extracellular sites of activity. Also, there will be less available protein to interact with Aβ peptide, thus enhancing its aggregation, which may explain the variant B cystatin C association with a higher risk of developing AD.

As the amyloid deposits are the histological hallmark of AD, drusen are the extracellular deposits found in AMD. The presence of Aβ peptide has been reported in patients with severe forms of AMD [55–58]. The involvement of protein aggregation in AMD pathogenesis is suggested by the presence of various toxic amyloid structures in drusen [56,59] and, indirectly, by the decrease in the AMD risk obtained through anti-amyloid treatment in a mouse model [60]. Variant B cystatin C aggregation may therefore contribute to AMD pathogenesis. In addition, if this mutation avoids the observed partnership between cystatin C and Aβ peptide it can account for the higher incidence of AD in homozygous patients. Further work is being carried out to investigate amyloid deposits formed by this variant inside RPE cells. More experimental approaches are necessary to reveal in full the mechanism of action of variant B cystatin C in these major degenerative diseases and we are actively pursuing such studies. With the actual lack of any *in vitro* aggregation experimental evidence to link the higher incidence of AD and AMD with variant B cystatin C, we believe that this study provides the important first clues for further investigations.

Acknowledgements

Conflict of interest

The authors declare no conflict of interest.

Author contribution

DF and LP conceived and supervised the study; RS, SV, DF and LP designed experiments; RS and SN performed experiments; LP and SV provided tools and reagents; RS, DF, LP, SN and SV analyzed data; RS, DF and LP wrote the manuscript; SV, LP and DF made manuscript revisions.

References

1 Grubb A and Löfberg H (1982) Human gamma-trace, a basic microprotein: amino acid sequence and presence in the adenohypophysis. *Proc Natl Acad Sci USA* **79**, 3024–3027.

2 Abrahamson M, Alvarez-Fernandez M and Nathanson C-M (2003) Cystatins. *Biochem Soc Symp* **70**, 179–199.

3 Turk V and Bode W (1991) The cystatins: protein inhibitors of cysteine proteinases. *FEBS Lett* **285**, 213–219.

4 Engh RA, Dieckmann T, Bode W, Auerswald EA, Turk V, Huber R and Oschkinat H (1993) Conformational Variability of Chicken Cystatin. *J Mol Biol* **234**, 1060–1069.

5 Tavéra C, Leung-Tack J, Prévot D, Gensac MC, Martinez J, Fulcrand P and Collé A (1992) Cystatin C secretion by rat glomerular mesangial cells: autocrine loop for in vitro growth-promoting activity. *Biochem Biophys Res Commun* **182**, 1082–1088.

6 Hasegawa A, Naruse M, Hitoshi S, Iwasaki Y, Takebayashi H and Ikenaka K (2007) Regulation of glial development by cystatin C. *J Neurochem* **100**, 12–22.

7 Bobek LA and Levine MJ (1992) Cystatins–inhibitors of cysteine proteinases. *Crit Rev Oral Biol Med* **3**, 307–332.

8 Warfel AH, Zucker-Franklin D, Frangione B and Ghiso J (1987) Constitutive secretion of cystatin C (gamma-trace) by monocytes and macrophages and its downregulation after stimulation. *J Exp Med* **166**, 1912–1917.

9 Lerner UH and Grubb A (2009) Human cystatin C, a cysteine proteinase inhibitor, inhibits bone resorption in vitro stimulated by parathyroid hormone and parathyroid hormone-related peptide of malignancy. *J Bone Miner Res* **7**, 433–440.

10 Yamada M (2000) Cerebral amyloid angiopathy: an overview. *Neuropathology* **20**, 8–22.

11 Grubb AO (2000) Cystatin C–properties and use as diagnostic marker. *Adv Clin Chem* **35**, 63–99.

12 Palsdottir A, Snorradottir AO and Thorsteinsson L (2006) Hereditary cystatin C amyloid angiopathy:

genetic, clinical, and pathological aspects. *Brain Pathol*
16, 55–59.

13 Palsdottir A, Helgason A, Palsson S, Bjornsson HT,
Bragason BT, Gretarsdottir S, Thorsteinsdottir U,
Olafsson E and Stefansson K (2008) A drastic
reduction in the life span of cystatin C L68Q carriers
due to life-style changes during the last two centuries.
PLoS Genet **4**, e1000099.

14 Nagai A, Kobayashi S, Shimode K, Imaoka K,
Umegae N, Fujihara S and Nakamura M (1998) No
mutations in cystatin C gene in cerebral amyloid
angiopathy with cystatin C deposition. *Mol Chem
Neuropathol* **33**, 63–78.

15 van Duinen SG, Castaño EM, Prelli F, Bots GT,
Luyendijk W and Frangione B (1987) Hereditary
cerebral hemorrhage with amyloidosis in patients of
Dutch origin is related to Alzheimer disease. *Proc Natl
Acad Sci USA* **84**, 5991–5994.

16 Sastre M, Calero M, Pawlik M, Mathews PM, Kumar
A, Danilov V, Schmidt SD, Nixon RA, Frangione B
and Levy E (2004) Binding of cystatin C to Alzheimer's
amyloid beta inhibits in vitro amyloid fibril formation.
Neurobiol Aging **25**, 1033–1043.

17 Mi W, Pawlik M, Sastre M, Jung SS, Radvinsky DS,
Klein AM, Sommer J, Schmidt SD, Nixon RA,
Mathews PM *et al.* (2007) Cystatin C inhibits amyloid-
beta deposition in Alzheimer's disease mouse models.
Nat Genet **39**, 1440–1442.

18 Gauthier S, Kaur G, Mi W, Tizon B and Levy E (2011)
Protective mechanisms by cystatin C in
neurodegenerative diseases. *Front Biosci (Schol Ed)* **3**,
541–554.

19 Paraoan L, Grierson I and Maden BE (2000) Analysis
of expressed sequence tags of retinal pigment
epithelium: cystatin C is an abundant transcript. *Int J
Biochem Cell Biol* **32**, 417–426.

20 Ida H, Boylan SA, Weigel AL, Smit-McBride Z, Chao
A, Gao J, Buchoff P, Wistow G and Hjelmeland LM
(2004) EST analysis of mouse retina and RPE/choroid
cDNA libraries. *Mol Vis* **10**, 439–444.

21 Wistow G, Bernstein SL, Wyatt MK, Fariss RN, Behal
A, Touchman JW, Bouffard G, Smith D and Peterson
K (2002) Expressed sequence tag analysis of human
RPE/choroid for the NEIBank Project: over 6000 non-
redundant transcripts, novel genes and splice variants.
Mol Vis **8**, 205–220.

22 Anderson DH, Mullins RF, Hageman GS and Johnson
LV (2002) A role for local inflammation in the
formation of drusen in the aging eye. *Am J Ophthalmol*
134, 411–431.

23 Booij JC, Baas DC, Beisekeeva J, Gorgels TGMF and
Bergen AAB (2010) The dynamic nature of Bruch's
membrane. *Prog Retin Eye Res* **29**, 1–18.

24 Mitter SK, Rao HV, Qi X, Cai J, Sugrue A, Dunn
WA, Grant MB and Boulton ME (2012) Autophagy in

the retina: a potential role in age-related macular
degeneration. *Adv Exp Med Biol* **723**, 83–90.

25 Kaarniranta K, Sinha D, Blasiak J, Kauppinen A,
Veréb Z, Salminen A, Boulton ME and Petrovski G
(2013) Autophagy and heterophagy dysregulation leads
to retinal pigment epithelium dysfunction and
development of age-related macular degeneration.
Autophagy **9**, 973–984.

26 Hua Y, Zhao H, Lu X, Kong Y and Jin H (2012)
Meta-analysis of the cystatin C(CST3) gene G73A
polymorphism and susceptibility to Alzheimer's disease.
Int J Neurosci **122**, 431–438.

27 Butler JM, Sharif U, Ali M, McKibbin M, Thompson
JP, Gale R, Yang YC, Inglehearn C and Paraoan L
(2015) A missense variant in CST3 exerts a recessive
effect on susceptibility to age-related macular
degeneration resembling its association with
Alzheimer's disease. *Hum Genet* **134**, 705–715.

28 Paraoan L, Hiscott P, Gosden C and Grierson I (2010)
Cystatin C in macular and neuronal degenerations:
Implications for mechanism(s) of age-related macular
degeneration. *Vision Res* **50**, 737–742.

29 Finckh U, von der Kammer H, Velden J, Michel T,
Andresen B, Deng A, Zhang J, Müller-Thomsen T,
Zuchowski K, Menzer G *et al.* (2000) Genetic
association of a cystatin C gene polymorphism with late-
onset Alzheimer disease. *Arch Neurol* **57**, 1579–1583.

30 Zurdel J, Finckh U, Menzer G, Nitsch RM and
Richard G (2002) CST3 genotype associated with
exudative age related macular degeneration. *Br J
Ophthalmol* **86**, 214–219.

31 Paraoan L, White MR, Spiller DG, Grierson I and
Maden BE (2001) Precursor cystatin C in cultured
retinal pigment epithelium cells: evidence for processing
through the secretory pathway. *Mol Membr Biol* **18**,
229–236.

32 Paraoan L, Grierson I and Maden BEH (2003) Fate of
cystatin C lacking the leader sequence in RPE cells.
Exp Eye Res **76**, 753–756.

33 Benussi L, Ghidoni R, Steinhoff T, Alberici A, Villa A,
Mazzoli F, Nicosia F, Barbiero L, Broglio L, Feudatari
E *et al.* (2003) Alzheimer disease-associated cystatin C
variant undergoes impaired secretion. *Neurobiol Dis* **13**,
15–21.

34 Paraoan L, Ratnayaka A, Spiller DG, Hiscott P, White
MRH and Grierson I (2004) Unexpected intracellular
localization of the AMD-associated cystatin C variant.
Traffic **5**, 884–895.

35 Conchillo-Solé O, de Groot NS, Avilés FX, Vendrell J,
Daura X and Ventura S (2007) AGGRESCAN: a
server for the prediction and evaluation of "hot spots"
of aggregation in polypeptides. *BMC Bioinformatics* **8**,
65.

36 Oliveberg M (2010) Waltz, an exciting new move in
amyloid prediction. *Nat Methods* **7**, 187–188.

37 Malmo C, Vilasi S, Iannuzzi C, Tacchi S, Cametti C, Irace G and Sirangelo I (2006) Tetracycline inhibits W7FW14F apomyoglobin fibril extension and keeps the amyloid protein in a pre-fibrillar, highly cytotoxic state. *FASEB J* **20**, 346–347.

38 Belli M, Ramazzotti M and Chiti F (2011) Prediction of amyloid aggregation in vivo. *EMBO Rep* **12**, 657–663.

39 Sánchez de Groot N, Pallarés I, Avilés FX, Vendrell J and Ventura S (2005) Prediction of "hot spots" of aggregation in disease-linked polypeptides. *BMC Struct Biol* **5**, 18.

40 Tsiolaki PL, Hamodrakas SJ and Iconomidou VA (2015) The pentapeptide LQVVR plays a pivotal role in human cystatin C fibrillization. *FEBS Lett* **589**, 159–164.

41 Tsiolaki PL, Louros NN, Hamodrakas SJ and Iconomidou VA (2015) Exploring the "aggregation-prone" core of human Cystatin C: A structural study. *J Struct Biol* **191**, 272–280.

42 Tsolis AC, Papandreou NC, Iconomidou VA and Hamodrakas SJ (2013) A consensus method for the prediction of "aggregation-prone" peptides in globular proteins. *PLoS One* **8**, e54175.

43 Reumers J, Maurer-Stroh S, Schymkowitz J and Rousseau F (2009) Protein sequences encode safeguards against aggregation. *Hum Mutat* **30**, 431–437.

44 Richardson JS and Richardson DC (2002) Natural beta-sheet proteins use negative design to avoid edge-to-edge aggregation. *Proc Natl Acad Sci USA* **99**, 2754–2759.

45 Sant'Anna R, Braga C, Varejão N, Pimenta KM, Graña-Montes R, Alves A, Cortines J, Cordeiro Y, Ventura S and Foguel D (2014) The importance of a gatekeeper residue on the aggregation of transthyretin: implications for transthyretin-related amyloidoses. *J Biol Chem* **289**, 28324–28337.

46 Fernandez-Escamilla A-M, Rousseau F, Schymkowitz J and Serrano L (2004) Prediction of sequence-dependent and mutational effects on the aggregation of peptides and proteins. *Nat Biotechnol* **22**, 1302–1306.

47 Iwata K, Fujiwara T, Matsuki Y, Akutsu H, Takahashi S, Naiki H and Goto Y (2006) 3D structure of amyloid protofilaments of beta2-microglobulin fragment probed by solid-state NMR. *Proc Natl Acad Sci USA* **103**, 18119–18124.

48 Byler DM and Susi H (1986) Examination of the secondary structure of proteins by deconvolved FTIR spectra. *Biopolymers* **25**, 469–487.

49 Barth A and Zscherp C (2002) What vibrations tell us about proteins. *Q Rev Biophys* **35**, 369–430.

50 Jackson M and Mantsch HH (1991) Protein secondary structure from FT-IR spectroscopy: correlation with dihedral angles from three-dimensional Ramachandran plots. *Can J Chem* **69**, 1639–1642.

51 Merz PA, Wisniewski HM, Somerville RA, Bobin SA, Masters CL and Iqbal K (1983) Ultrastructural morphology of amyloid fibrils from neuritic and amyloid plaques. *Acta Neuropathol* **60**, 113–124.

52 Bitan G, Kirkitadze MD, Lomakin A, Vollers SS, Benedek GB and Teplow DB (2003) Amyloid beta - protein (Abeta) assembly: Abeta 40 and Abeta 42 oligomerize through distinct pathways. *Proc Natl Acad Sci USA* **100**, 330–335.

53 Ferreira N, Saraiva MJ and Almeida MR (2011) Natural polyphenols inhibit different steps of the process of transthyretin (TTR) amyloid fibril formation. *FEBS Lett* **585**, 2424–2430.

54 Ferreira N, Saraiva MJ and Almeida MR (2012) Natural polyphenols as modulators of TTR amyloidogenesis: in vitro and in vivo evidences towards therapy. *Amyloid* **19** (Suppl 1), 39–42.

55 Dentchev T, Milam AH, Lee VM-Y, Trojanowski JQ and Dunaief JL (2003) Amyloid-beta is found in drusen from some age-related macular degeneration retinas, but not in drusen from normal retinas. *Mol Vis* **9**, 184–190.

56 Luibl V, Isas JM, Kayed R, Glabe CG, Langen R and Chen J (2006) Drusen deposits associated with aging and age-related macular degeneration contain nonfibrillar amyloid oligomers. *J Clin Invest* **116**, 378–385.

57 Anderson DH, Talaga KC, Rivest AJ, Barron E, Hageman GS and Johnson LV (2004) Characterization of beta amyloid assemblies in drusen: the deposits associated with aging and age-related macular degeneration. *Exp Eye Res* **78**, 243–256.

58 Johnson LV, Leitner WP, Rivest AJ, Staples MK, Radeke MJ and Anderson DH (2002) The Alzheimer's A beta -peptide is deposited at sites of complement activation in pathologic deposits associated with aging and age-related macular degeneration. *Proc Natl Acad Sci USA* **99**, 11830–11835.

59 Isas JM, Luibl V, Johnson LV, Kayed R, Wetzel R, Glabe CG, Langen R and Chen J (2010) Soluble and mature amyloid fibrils in drusen deposits. *Invest Ophthalmol Vis Sci* **51**, 1304–1310.

60 Ding J-D, Johnson LV, Herrmann R, Farsiu S, Smith SG, Groelle M, Mace BE, Sullivan P, Jamison JA, Kelly U et al. (2011) Anti-amyloid therapy protects against retinal pigmented epithelium damage and vision loss in a model of age-related macular degeneration. *Proc Natl Acad Sci USA* **108**, E279–E287.

61 Kolodziejczyk R, Michalska K, Hernandez-Santoyo A, Wahlbom M, Grubb A and Jaskolski M (2010) Crystal structure of human cystatin C stabilized against amyloid formation. *FEBS J* **277**, 1726–1737.

62 Bode W, Engh R, Musil D, Thiele U, Huber R, Karshikov A, Brzin J, Kos J and Turk V (1988) The 2.0 A X-ray crystal structure of chicken egg white cystatin and its possible mode of interaction with cysteine proteinases. *EMBO J* **7**, 2593–2599.